RSC Advances

ROYAL SOCIETY OF CHEMISTRY

www.rsc.org/advances

Highly dispersed graphene ribbons produced from ZnO/C core–shell nanorods and their use as a filler in polyimide composites

Hossain Shima,[a] Muhammad Mohsin Hossain,[a] Jae Ryang Hahn[a,b,*]

[a]*Department of Chemistry and Bioactive Material Sciences and Research Institute of Physics and Chemistry, Chonbuk National University, Jeonju 561–756, Korea*

[b]*Textile Engineering, Chemistry and Science, North Carolina State University 2401 Research Dr. Raleigh, NC 27695–8301, USA*

[*]Corresponding author: Tel: +82-63-270-3410. E-mail: jrhahn@jbnu.ac.kr (Jae R. Hahn)

ABSTRACT

Long and few–layer thickness graphene ribbons (GRs) were fabricated through an efficient process from a well–ordered array of ZnO/C core–shell hexagonal nanorods that were formed by thermally heating zinc acetate dihydrate in a sealed chamber. The lengths and widths of the GRs were as high as ~50 μm and 100–400 nm, respectively. The GRs could be highly dispersed (~2 mg/mL) in 1-methyl-2-pyrrolidinone and exhibited a good electrical conductivity (5,107 S/m). The highly dispersed and highly conductive GRs were applied to the fabrication of a GR–polyimide composite film that exhibited good mechanical properties while preserving the film transparency.

Keywords: graphene ribbons, high dispersion concentration, electrical conductivity, ZnO/C core–shell nanorods, polyimide composite

1. INTRODUCTION

Graphene layers display an outstanding carrier mobility at room temperature,[1] a good thermal conductivity,[2,3] a high modulus and tensile strength,[4] and a high transparency[5,6] toward incident light over a broad wavelength range. The excellent electronic, thermal, and mechanical properties of graphene are useful in certain electronic devices; however, the zero band gap of semimetal graphene generally gives a low switching ratio in graphene–based devices and restricts the applicability of graphene in electronics. Significant efforts have been applied toward increasing the band gap in graphene's density of states. One approach has involved cutting graphene layers into narrow ribbons to induce quantum confinement effects.

In practice, two characteristics of graphene ribbons (GRs) are needed for device applications. First, high–quality GRs must be produced in large scale. Several strategies for mass producing high–quality narrow GRs have been developed based on the unzipping of carbon nanotubes (CNTs), plasma etching,[7] metal–catalyzed cutting,[8] laser irradiation,[9] or hydrogen treatment with annealing.[10] All approaches used solid substrates as a template for GR fabrication; therefore, additional processing was needed, for example separation from the substrate to obtain the solution–phase GR. Chemical etching or high–temperature heating steps were applied to facilitate separation from the substrate. These additional processes reduce the compatibility of the GRs with other device components. The utility of GRs could be improved by preparing them through CNT unzipping or graphene cutting processes carried out in solution;[11–16] however, the yields of these processes do not exceed 60%. A high effective yield (80–100%) was obtained by chemically breaking down CNTs in the presence of a 500 wt% oxidizing agent ($KMnO_4$) solution. This approach is poorly compatible with industrial synthesis processes due to the high quantity of oxidizing agent. A variety of chemicals have been tested for their ability to reduce the

oxidized GRs.[17] It is interesting that Pd nanorods could be used to produce GRs.[18] Plasma enhanced chemical vapor deposition of graphene was carried out on Pd nanorods, which could produce GRs with a width of 100–250 nm and a thickness of 1–30 layers. None of these approaches were found to be suitable for large–scale synthesis procedures due to incompatibilities with substrates. Most chemical synthesis approaches require high temperatures and/or catalysts, and they tend to involve many steps. The second requirement is that GRs must be readily dispersed in a liquid phase to enable the use of GRs in devices and to control the thicknesses of films prepared on a variety of substrate types. Highly dispersed and highly concentrated conductive carbon materials in a liquid phase are useful as electron acceptors, in hole transport layers,[19] and as counter electrodes.[20]

This paper describes an efficient novel method for fabricating a stack of long (~50 μm long) narrow (100–400 nm wide) GRs from a solid array of ZnO/C core–shell hexagonal nanorods produced through a thermolysis process in a sealed homemade reactor (**Fig. 1**). This procedure carried out without the use of a substrate or a catalyst. The carbon shell layers of ZnO/C core–shell nanorods were stripped off using acid treatment over a short period of time (5 min) and then converted to GRs by solution sonication. The electrical conductivity of the ZnO/C core–shell hexagonal nanorods and few layer GRs were measured. A practical application of a solution comprising the highly dispersed GRs was demonstrating by fabricating GR–polyimide (GR–PI) composites that exhibited excellent mechanical properties. The strong interactions between the long GRs and the polymer enhanced the tensile strength and Young modulus of the GR–PI composite relative to the values obtained from the pure PI film by 54.8% and 156%, respectively.

2. EXPERIMENTAL SECTION

2.1. Chemicals

Zinc acetate dihydrate (99%, Sigma Aldrich), hydrochloric acid (37%, Sigma Aldrich), *n*-methyl-2-pyrrolidone (NMP, Sigma Aldrich), ethanol (Samchun Chemicals, 99.5%), 4,4'-oxydianiline (ODA, Sigma Aldrich), and pyromellitic dianhydride (PMDA, Sigma Aldrich) were used as received.

2.2. Instruments

The structures of the products were characterized by collecting multi–purpose high–performance X–ray diffraction patterns (XRD, X'pert Powder, Analytical). Scanning electron microscopy (SEM) images were obtained using a JEOL JSM–6400 microscope under an accelerating voltage of 0.2–40 kV, 0.2–5 kV (in 100 V steps), and 5–40 kV (in 1 kV steps). X–ray energy–dispersive spectroscopy (EDX, Horiba, EMAX) was used in conjunction with FE–SEM (S–4700, Hitachi, Japan) to characterize the chemical constituents of the materials. Transmission electron microscopy (TEM) measurements were obtained using a JEOL JEM–2010 microscope. The Raman spectra (using a HORIBA JOBIN YVON, Lab RAM HR, Laser 514.54 nm) were collected to characterize the vibrational characteristics of the GRs. The electrical conductivity of the ZnO/C core–shell hexagonal nanorods and GRs were measured using a four–point probe instrument (FPP–RS8, DasolEng, Korea). A Universal Testing Machine (UTM 5567A, INSTRON, USA) was used to characterize the mechanical properties of the GR–PI composites.

2.3. Fabrication of a solid array of ZnO/C core–shell hexagonal nanorods

Zinc acetate dihydrate (1 g) was placed in a home–built stainless steel reactor (SUS 316, volume of 7.7 cm^3), which was then sealed with a copper gasket (OFHC). The reactor was

placed in the chamber of a muffle–type furnace prepared using high–purity fibrous alumina. The temperature was controlled using a programmable silicon–controlled rectifier. Solid arrays of ZnO/C core–shell nanorods were fabricated by heating the reactor to 450°C over 40 h. After thermolysis, the reactor was slowly cooled to room temperature under programmed control over 5 h. The dark products were collected and separated into two parts. One part was washed with ethanol and then annealed at 100°C for 2 h for characterization. A fine powder of the product was characterized using XRD, SEM, EDX, and TEM techniques.

2.4. Synthesis of a stack of the GRs

The other portion of the above ZnO/C core–shell hexagonal nanorod sample was treated with 10% HCl acid, followed by bath sonication for 5 min. The ZnO portion of the nanorods was dissolved in HCl to produce $ZnCl_2$ in an aqueous phase. This phase was separated by filtration, and the GRs remained as a precipitate. The few layer GRs were washed several times by deionized water to remove acid and other impurities. The GR black powder was dried at 100°C for 2 h and characterized by XRD, SEM, EDX, TEM, and Raman spectroscopy. The electrical conductivity could be improved by heating the GRs in a stainless steel reactor for 40 min at 500°C in a sealed nitrogen environment. The temperature was varied slowly at a rate of 5°C/min. The Raman spectra and electrical conductivity properties of this compound were then measured.

2.5. Electrical conductivity properties of the ZnO/C core–shell hexagonal nanorods and GRs

A disk of the ZnO/C core–shell nanorods was prepared using a CrushIR press (Digital Hydraulic press, PIKE Technologies, USA). An 80 mg sample of the ZnO/C core–shell nanorods was pressed under a force of 14 US tons to prepare a disk 260 μm thick. Similarly, a GR disk was prepared by pressing 50 mg of the sample to form a 220 μm thick disk. The surface

electrical conductivities of the disks were measured using a four–point probe instrument. The resistances of the ZnO/C core–shell nanorods and the GRs were ~70 Ω/sq and ~890 mΩ/sq, respectively.

2.6. Fabrication of the GR–PI composite

A 0.1 wt% GR–PI composite film was produced by adding GRs (4 mg) to the NMP solvent (20 mL), and the solution was sonicated for 1 h. ODA (2 g) was then added to the GR solution, which was stirred for 25 min. PMDA (2.16 g) was added and the solution was stirred for 30 min in an ice bath and then for 24 h at room temperature to produce a GR–polyamic acid (GR–PAA) composite. The GR–PAA composite solution was poured over a clean pure PI film for bar–cast coating. The bar–cast GR–PAA film prepared on the pure PI film was heated at 90°C for 2 h under vacuum to produce a GR–PAA composite film. After vacuum heating, the GR–PAA film was separated from the commercial PI film and was further heated at 350°C over 4 h to produce a GR–PI film. The same approach was used to prepare 0.5 wt% and 1 wt% GR–PI composite films.

3. RESULTS AND DISCUSSION

3.1. Formation of a solid array of ZnO/C core–shell nanorods

The ZnO/C core–shell nanorods were characterized by XRD to identify the composition of the sample (**Fig. S1**). The as–prepared products prior to acid treatment (**Fig. S1a)** displayed peaks corresponding to several crystal planes of ZnO (JCPDS No. 01-075-0576), in good agreement with the peaks observed from a standard wurtzite ZnO sample (space group: p63mc (186), a=0.325 nm, c=0.5207 nm). No other phases or impurities were detected in this spectrum. Carbon of (002) plane was weakly observed at 24.37° (inset in **Fig. S1a**), which is possibly due

to the formation of an amorphous carbon shell around the ZnO core. Carbon was also detected in the EDX spectrum of the ZnO/C core–shell nanorods (**Fig. S2a**), confirming that these nanorods were composed of Zn, O, and C. A well–aligned and stepped array of ZnO/C core–shell nanorods was observed by SEM (**Fig. 2**). Larger–scale SEM images (**Fig. 2a**) revealed a stepped array of ZnO/C core–shell nanorods that was aligned well along one direction. The image of a single nanorod revealed the hexagonal shapes of the rods (**Fig. 2b**), which terminated in a hexagonal pyramidal shape. **Figure 2c** shows the front view of tip portion of hexagonal nanorods. **Figures 2d and 2e** show the SAED patterns and HR–TEM images, respectively, obtained from a few of the ZnO/C core–shell hexagonal nanorods. The SAED patterns revealed that the hexagonal nanorods were composed of single crystalline ZnO. A 2.6 Å {0002} lattice fringe was observed parallel to the basal plane. A 2.81 Å {1100} lattice fringe and a single crystal {1100} zone–axis diffraction pattern were also observed. High–resolution TEM images of the nanorods **(Fig. 2e**) clearly revealed the presence of a carbon layer (transparent phase) deposited on the surfaces of the ZnO nanorods.

3.2. Formation of the GRs: highly dispersed and stable

Acid treatment of the ZnO/C core–shell nanorods (10% HCl acid) produced the GRs in an insoluble phase. The insoluble phase was dried in an oven at 100°C for 2 h. The GRs compositions were analyzed using XRD, EDX, and Raman spectroscopy. The XRD spectrum displayed a broad carbon peak of (002) plane at 25.84° (inset in **Fig. S1b**). The GRs contained oxidized carbon, as revealed by the EDX analysis (**Fig. S2b**), indicating that the carbon was oxidized during the synthesis process. No zinc peak was present. These results indicated that the ZnO was perfectly separated from the ZnO/C core–shell materials. The Raman spectra of the as–prepared GRs (**Fig. 3a**) displayed a D band, indicating the presence of some defects. The sp^2

carbon centers were probably converted to sp^3 carbon centers through oxidation during the synthesis process. The defect density in the GRs could be reduced by heating the as–prepared GRs at 500°C for 40 min in a sealed environment under a nitrogen atmosphere. The low I_D/I_G ratio obtained from the heated GRs (**Fig. 3b**), 0.37, relative to the ratio obtained from the non–heated GRs (0.73), indicated that the reduction reaction occurred during the heating process. Two–dimensional peaks obtained from both GR samples were observed at 2725.29 cm^{-1}.

In order to characterize the thickness of GRs, the intensity and the full width at half maximum (FWHM) of 2D band of Raman spectra were analyzed.[21-24] The I_{2D}/I_G (or I_G/I_{2D}) and FWHM of 2D band of the spectrum shown in Fig. 3 were 1.47 (or 0.68) and 0.48 cm^{-1}, respectively. Raman spectra taken from several GRs (marked in the optical image) are further shown in Fig. S3. Fig. S3b, taken at position 1, shows the I_{2D}/I_G (or I_G/I_{2D}) of 0.72 (or 1.45) and FWHM of 62 cm^{-1}. The Raman spectra obtained at positions 2 and 3 exhibited the similar values to those of Fig. 3. These indicate that the Raman spectra shown in Fig. 3 and Fig. S3b were obtained from bi-layer and tri-layer GRs, respectively. These features are also similar to those of graphenes produced by thermal activation of pristine graphites.[25] Our analysis shows that the GRs obtained in this work is a mixture of bi- and tri-layer GRs.

Figure 4 shows the shapes and dimension of the GRs. SEM images (**Figs. 4a–c**) of graphene revealed a stack of thin and long GRs. **Fig. 4c** shows the magnified area of the marked rectangle in **Fig. 4b**. The lengths of these stacks were ~50 μm. TEM images of the GRs (**Fig. 4d**) also indicated that the sheets were transparent and thin. The inset in **Fig. 4d** shows the selected–area electron diffraction pattern featuring a ring pattern corresponding to an amorphous carbon phase of as–prepared GRs. Individual GRs are shown in **Fig. 4e and Fig. 4g**. The HR–TEM images (**Fig. 4f and Fig. 4h**) indicated the presence of tri- and by–layer thickness GRs, which is

consistent with analysis of Raman spectra.

It is interesting that the widths of the GRs were 100–400 nm. The carbon layer on ZnO/C core-shell rods is amorphous, which is concluded based on XRD, EDX, and diffraction results. Sonication of ZnO/C core–shell rods in 10% HCl allows HCl react with core ZnO and attack the carbon layer selectively along the amorphous region in which Zn (or other functional group) may be connected with carbon.[26] It is possible that the amorphous region is randomly distributed along the layer. Unzipping of carbon layer would then be carried out selectively along the more amorphous carbon region. This can eventually result in a distribution of inhomogeneous lateral widths of GRs.

The SEM image revealed a tube structure composed of a carbon shell (**Fig. 5a**). Few of the CNTs were found to undergo unzipping after only 3 min sonication. More unzipping was observed after 4 min sonication (**Fig. 5b**). After 5 min sonication, the products were found to be completely unzipped (**Fig. 5c**). The tubes can be collapsed or broken or unzipped possibly due to the amorphous carbon which is chemically bonded with Zn as a form of Zn–OOC–CNT (carbon shell layer) or Zn–OCNT (carbon shell layers).[26] The peak at 24.37° of carbon (002) plane of ZnO/C core–shell, which is shifted from that of GRs (25.84°) in XRD (**Fig. S1**), indicates a chemical bond between carbon shell and ZnO core. Due to this chemical bonding the *d*–space of carbon shell may increase.

Based on the SEM images of the few layer GRs, a schematic of the GR growth mechanism could be proposed, as illustrated in **Figs. 6a–f**. **Figure 6b** shows the tube structure of the carbon shell layer prepared from the ZnO/C core–shell hexagonal nanorods (**Fig. 6a**) after dissolution of the inner ZnO core in the presence of HCl acid. The CNT (**Fig. 6b**) was unzipped (**Figs. 6c–e**) during the sonication at room temperature. The unzipped CNT (**Fig. 6e**) was further split and

converted to GRs (**Fig. 6f**).

The GRs were readily dispersed in an organic solvent and could be highly concentrated to form a stable dispersion. These physical properties were crucial for the synthesis of polyimide polymer composites and devices. The properties of the NMP–based GR dispersion were tested (**Figs. 6g and 6h)**. The dispersion concentration of GRs in NMP solvent was measured as following. A 200 mg sample of the heated GRs was dissolved in 20 mL NMP, followed by sonication for 10 min at 40% amplitude using a Sonics Vibra Cell CV 334 (USA). The dispersion was then allowed to settle for two weeks. All GRs primarily dissolved in the NMP solvent. Precipitation occurred slowly after one week and was separated from the top 80% of the layer after two weeks. The top 80% of the layer (4 mL) was taken in a Petri dish, then solvent was evaporated from GRs solution at 200°C for 1 h and 350°C for 4 h to completely evaporate solvent. The weight of the dried precipitate was measured. The suspended GRs was 7.8 mg in 4 mL NMP solvent (1.95 mg/mL). Stability of GRs in NMP was further tested by allowing the top 80% layer to settle for another three months. After three months, the concentration was found to be 1.95 mg/mL. This dispersion concentration was very high compared to other types of carbon materials, as summarized in **Table 1**.[27–33]

3.3. Electrical conductivity of the ZnO/C core–shell nanorods and the GRs

The electrical conductivity of the ZnO/C core–shell hexagonal nanorods in pellet form was measured to be 55 S/m using a four–point probe instrument. This conductivity was relatively high compared to the values obtained from other metal–metal oxide composites or core–shell materials (**Table S1**)[34–36] due to the properties of the carbon layer. A high electrical conductivity in a metal oxide can play an important role in improving the sensing performance of a sensor by decreasing the amount of conductive composite filler and by increasing the conductivity of the

metal oxide composite and electric wire. The nanorods prepared here may be useful for preparing high–performance supercapacitor electrodes,[37] dye–sensitized solar cells,[38] and gas sensors. The GRs displayed a good surface electrical conductivity (5107 S/m, measured by four–point probe technique) compared to other carbon materials, as summarized in **Table S2**.[27,28,31,36,39–44] A high electrical conductivity in a carbon material is crucial for the preparation of supercapacitors, sensors, energy storage devices,[40, 45] or conducting polymer composites.[46]

3.4. Use of the GRs as a filler in a polymer composite

As an example application, the concentrated and highly dispersed GRs were used as a filler in combination with a polyimide composite. ODA was added to the GR–NMP solution with stirring.[46] PMDA was then added to this solution with stirring in an ice bath to produce a GR–PAA composite. The GR–PAA composite solution was poured onto a clean pure PI film for bar–cast coating. The bar–cast GR–PAA layer on the pure PI film was heated under vacuum to produce a GR–PAA composite film (**Fig. 7a**). The GR–PAA film was heated at 350°C for 4 h to fabricate a GR–PI film (**Fig. 7b**). The mechanical properties of the fabricated films were tested by measuring the stress versus strain curves of the films formed from pure PI or GR–PI composites in various wt% (**Fig. 7c**). The stress and Young modulus of the pure PI film were 84.3 MPa and 1.2 GPa, respectively. The stress and Young modulus of the GR–PI composite film improved to 130.5 MPa and 3.08 GPa, respectively, at 1 wt% (**Table 2**). Even at a very low filler content (1 wt%), the mechanical properties of the film were much better than those obtained from other polymer composite films (**Table 3**).[47–52] A 1 wt% GR–PI film displayed a higher stress and Young modulus, values that were 54.8% and 156%, respectively, of the values obtained from other polymer composites. The transparency of a film generally decreases as the carbon filler content in the PI film is increased. Therefore, low graphene content is important for

preparing highly transparent devices.

The EDX (**Fig. S2**) and Raman spectra (**Fig. 3 and Fig. S3**) of the GRs indicated that the GRs included defects. Defects in the carbon materials were most likely due to hydroxyl (–OH), carboxylic (–COOH), and epoxy (–O–) groups, or to non–conjugated double bonds. Hydrogen bonds between the partially positive hydrogen atoms on the $–NH_2$ groups in the PI and the partially negative oxygen atoms on the –OH or –COOH groups in the GRs may also have contributed to the defect centers. The length of the GRs and presence of hydrogen bonds are crucial for enhancing the mechanical properties of the GR–PI composite films. TEM image (**Fig. 4d**) also shows that the GRs are interconnected, which may contribute to the improvement of mechanical properties of GR–PI composite. The GR–PI polymer composite prepared here, which showed excellent mechanical properties, may be applicable to aerospace devices,[48] supercapacitors, and nanoelectronic devices.[53]

4. CONCLUSIONS

We demonstrated the preparation of an environmentally friendly a novel and efficient method for fabricating stacks of long and few–layer thickness GRs from a well–ordered array of ZnO/C core–shell structures. Zinc acetate dihydrate was sealed in a solvent–free sealed reactor without any catalyst or template under a nitrogen environment. The carbon shell layers of the ZnO/C core–shell nanorods were effectively isolated as GRs in the solution phase after a short period of HCl treatment. Furthermore, the separated GRs dissolved in the NMP solvent in a high concentration (~2 mg/mL) without any surfactant, ionic liquid, or stabilizer. The high dispersion concentration in the liquid phase was useful for improving the mechanical properties of the PI

film. The GR–PI polymer composite film displayed an excellent Young modulus and stress value relative to the values obtained from a pure PI film.

ACKNOWLEDGMENTS

This work was supported by grants from the Korean government (NRF, MSIP, 2010–0024254 and 2007–0056095).

REFERENCES

1. C. Berger, Z. Song, X. Li, X. Wu, N. Brown, C. Naud, D. Mayou, T. Li, J. Hass, A. Marchenkoy, E. Conrad, P. First and W. de Heer, *Science,* 2006, **312**, 1191–1196.
2. A. A. Balandin, S. Ghosh, W. Bao, I. Calizo, D. Teweldebrhan, F. Miao and C. N. Lau, *Nano Lett*., 2008, **8**, 902–907.
3. S. Ghosh, I. Calizo, D. Teweldebrhan, E. P. Pokatilov, D. L. Nika, A. A. Balandin, W. Bao, F. Miao and C. N. Lau, *Appl. Phys. Lett*., 2008, **92**, 151911.
4. C. Lee, X. Wei, J. W. Kysar and J. Hone, *Science*, 2008, **321**, 385–388.
5. R. R. Nair, P. Blake, A. N. Grigorenko, K. S. Novoselov, T. J. Booth and T. Stauber, *Science*, 2008, **320**, 1308–1311.
6. S. Bae, H. Kim, Y. Lee, X. Xu, J–S. Park, Y. Zheng, J. Balakrishnan, T. Lei, H. R. Kim, Song, I. Young, Y–J. Kim, K. S. Kim, B. Oezyilmaz, J–H. Ahn, B. H. Hong and S. Iijima, *Nat Nanotechnol*., 2010, **5**, 574–578.
7. L. Jiao, L. Zhang, X. Wang, G. Diankov and H. Dai, *Nature*, 2009, **458**, 877–880.
8. A. L. Elias, A. R. Botello–Mendez, D. Meneses–Rodriguez, V. J. Gonzalez, D. Ramirez–Gonzalez and L. Ci, *Nano Lett*., 2010, **10**, 366–372.
9. P. Kumar, L. S. Panchakarla and C. N. R. Rao, *Nanoscale*, 2011, **3**, 2127–2129.
10. A. V. Talyzin, S. Luzan, I. V. Anoshkin, A. G. E. Nasibulin and H. E. I. J. Kauppinen, *ACS Nano*, 2011, **5**, 5132–5140.
11. X. Li, X. Wang, L. Zhang, S. Lee and H. Dai, *Science*, 2008, **319**, 1229–1232.
12. A. G. Cano–Marquez, F. J. Rodriguez–Macias, J. Campos–Delgado, C. G. Espinosa–Gonzalez, F. Tristan–Lopez and D. Ramirez–Gonzalez, *Nano Lett*., 2009, **9**, 1527–1533.

13. D. V. Kosynkin, W. Lu, A. Sinitskii, G. Pera, Z. Sun and J. M. Tour, *ACS Nano*, 2011, **5**, 968–974.

14. L. Jiao, X. Wang, G. Diankov, H. Wang and H. Dai, *Nat Nanotechnol*., 2010, **5**, 321–325.

15. L. Xie, H. Wang, C. Jin, X. Wang, L. Jiao, K. Suenaga and H. Dai, *J. Am. Chem. Soc*., 2011, **133**, 10394–10397.

16. D. B. Shinde, J. Debgupta, A. Kushwaha, M. Aslam and V. K. Pillai, *J. Am. Chem. Soc*., 2011, **133**, 4168–4171.

17. J. Cai, P. Ruffieux, R. Jaafar, M. Bieri, T. Braun and S. Blankenburg, *Nature,* 2010, **466**, 470–473.

18. J. Y. Woo, H. C. Sang, P. David, Y. L. Si, H. H. Gang, Y. Minhee and H. L. Young, *ACS Nano*, 2010, **4**, 5480–5486.

19. S. S. Li, K. H. Tu, C. C. Lin, C. W. Chen and M. Chhowalla, *ACS Nano*, 2010, **4**, 3169–3174.

20. L. Kavan, J. H. Yum and M. Gratze, *Nano Lett*., 2011, **11**, 5501–5506.

21. Z. Peng, Z. Yan, Z. Sun and J. M. Tour, *ACS Nano,* 2011, **5**, 8241–8247.

22. S. Chen,W. Cai, R. D. Piner, J. W. Suk, Y. Wu, Y. Ren, J. Kang and R. S. Ruoff, *Nano Lett.,* 2011, **11**, 3519–3525.

23. Z. Sun, Z. Yan, J. Yao, E. Beitler, Y. Zhu and J. M. Tour, *Nature,* 2010, **468**, 549–552.

24. L. Xuesong, C. Weiwei, A. Jinho, K. Seyoung, N. Junghyo, Y. Dongxing, P. Richard, V. Aruna, J. Inhwa , T. Emanuel, B. K. Sanjay, C. Luigi and R. S. Ruoff, *Science,* 2009, **324,** 1312–1314.

25. M. M. Hossain, O. K. Park, J. R. Hahn and B. C. Ku, *Mater. Lett.*, 2014, **123**, 90–92.

26. D. I. Son, B. W. Kwon, D. H. Park, W. S. Seo, Y. Yi, B. Angadi, C. L. Lee and W. K. Choi, *Nat. Nanotechnol*., 2012, **7**, 465–471.

27. Y. Hernandez, V. Nicolosi, M. Lotya, F. M. Blighe, Z. Y. Sun, S. De, I. T. McGovern, B. Holland, M. Byrne, Y. K. Gun'ko, J. J. Boland, P. Niraj, G. Duesberg, S. Krishnamurthy, R. Goodhue, J. Hutchison, V. Scardaci, A. C. Ferrari and J. N. Coleman, *Nat. Nanotechnol.,* 2008, **3**, 563–568.

28. C. E. Hamilton, J. R. Lomeda, Z. Sun, J. M. Tour and A. R. Barron, *Nano Lett*., 2009, **9**, 3460–3462.

29. A. A. Green and M. C. Hersam, *Nano Lett*., 2009, **9**, 4031–4036.

30. M. Lotya, Y. Hernandez, P. J. King, R. J. Smith, V. Nicolosi, L. S. Karlsson, F. M. Blighe, S. De, W. Wang, I. T. McGovern, G. S. Duesberg and J. N. Coleman, *J. Am. Chem. Soc*., 2009, **131**, 3611–3620.

31. D. Li, M. B. Muller, S. Gilje, R. B. Kaner and G. G. Wallace, *Nat. Nanotechnol.,* 2008, **3**, 101–105.

32. X. Wang, P. F. Fulvio, G. A. Baker, G. M. Veith, R. R. Unocic, S. M. Mahurin, M. Chi, and S. Dai, *Chem. Commun.,* 2010, **46**, 4487–4489.

33. N. Behabtu, J. R. Lomeda, M. J. Green, A. L. Higginbotham, A. Sinitskii, D. V. Kosynkin, D. Tsentalovich, A. N.G. Parra-Vasquez, J. Schmidt, E. Kesselman, Y. Cohen, Y. Talmon, J. M. Tour and M. Pasquali, *Nat. Nanotechnol.,* 2010, **5**, 406–411.

34. Y. Fan, W. Jiang and A. Kawasaki, *Adv. Funct. Mater.,* 2012, **22**, 3882–3889.

35. E. Flahaut, A. Peigney, Ch. Laurent, Ch. Marliere, F. Chastel and A. Rousset, *Acta. Mater*., 2000, **48**, 3803–3812.

36. M. M. Hossain, A. H. A. Mamun and J. R. Hahn, *J. Phys. Chem. C,* 2012, **116**, 23153–23159.

37. L. Bao, J. Zang and X. Li, *Nano Lett*., 2011, **11**, 1215–1220

38. M. Law, L. K. Greene, A. Radenovic, T. Kuykendall, J. Liphardt and P. Yang, *J. Phys. Chem. B*, 2006, **110**, 22652–22663.

39. H. J. Shin, K. K. Kim, A. Benayad, S. M. Yoon, H. K. Park, I. S. Jung, M. H. Jin, H–K. Jeong, J. M. Kim, J–Y. Choi and Y. H. Lee, *Adv. Funct. Mater*., 2009, **19**, 1987–1992.

40. M. A. Worsley, P. J. Pauzauskie, T. Y. Olson, Y. Tammy, J. Biener, J. H. Satcher and T. F. Baumann, *J. Am. Chem. Soc*., 2010, **132**, 14067–14069.

41. S. Stankovich, D. A. Dikin, R. D. Piner, K. A. Kohlhaas, A. Kleinhammes, Y. Jia, Y. Wu, S. B. T. Nguyen and R. S. Ruoff, *Carbon*, 2007, **45**, 1558–1565.

42. Y. Si and E. T. Samulski, *Nano Lett*., 2008, **8**, 1679–1682.

43. Z. J. Fan, W. Kai, J. Yan, T. Wei, L. J. Zhi, J. Feng, Y–M. Ren, L–P. Song and F. Wei, *ACS Nano*, 2011, **5**, 191–198.

44. L. L. Zhang, X. Zhao, M. D. Stoller, Y. J. H. Zhu, S. Murali, Y. Wu, S. Perales, B. Clevenger and R. S. Ruoff, *Nano Lett*., 2012, **12**, 1806–1812.

45. L. Hua, J. W. Choia, Y. Yanga, S. Jeongb, F. L. Mantiaa, Li–F. Cuia and Y. Cuia, *Proc. Natl. Acad. Sci.* 2009, **106**, 21490–21494.

46. M. M. Hossain, J. R. Hahn and B. –C. Ku, *Bull. Korean Chem. Soc.,* 2014, **35**, 2049–2056.

47. N. D Luong, U. Hippi, J. T. Korhonen, A. J. Soininen, J. Ruokolainen, L-S. Johansson, J-D. Nam, L. H. Sinh and J. Seppala, *Polymer*, 2011, **52**, 5237–5242.

48. T. Huang, R. Lu, C. Su, H. Wang, Z. Guo, P. Liu, Z. Huang, H. Chen and T. Li, *ACS Appl. Mater. Interfaces,* 2012, **4**, 2699–2708.

49. D. Chen, H. Zhu and T. Liu, *ACS Appl. Mater. Interfaces,* 2010, **2**, 3702–3708.

50. G. Y. Kim, M. C. Choi, D. Lee and C. S. Ha, *Macromol. Mater. Eng*., 2012, **297**, 303–311.

51. M. Yoonessi, Y. Shi, D. A. Scheiman, M. L. Colon, D. M. Tigelaar, R. A. Weiss and M. A. Meador, *ACS Nano,* 2012, **6**, 7644–7655.

52. S. Peter, W. Rainer, T. Ralf and M. Rolf, *Macromol. Rapid Commun.*, 2009, **30**, 316–327

53. S. Wang, P. K. Ang, Z. Wang, A. L. L. Tang, J. T. L. Thong and K. P. Loh, *Nano Lett*., 2010, **10**, 92–98.

Table 1. Concentrations of the dispersion prepared from various carbon materials.

Carbon types	Solvent	Dispersion concentration (mg/ml)	Thickness
Graphene[27]	NMP	0.01	Mono-, bi-, and multi-layer
Graphene[28]	ODCB	0.02-0.03	Mono-, bi-, and multi-layer
Graphene[29]	Sodium chlorate	0.09-0.25	N/A
Graphene[30]	Water	0.1	Mono and multi-layer
Graphene[31]	Water	0.5	N/A
Graphene[32]	Ionic liquid	0.95	Multi-layer
Graphene[33]	Chlorosulfonic acid	2	Mono and multi-layer
GRs (our work)	**NMP**	**1.95**	**Few layer**

ODCB: orthodichloro benzene; Ionic liquids : 1-butyl-3-methylimidazolium bis(trifluoro-methane-sulfonyl)imide ([Bmim]-[Tf2N]).

Table 2. Mechanical properties of the GR–PI composite, prepared in various wt%.

Materials	Filler–Wt%	Stress (MPa)	Strain (%)	Young Modulus (GPa)
Pure Polyimide	0	84.3±13	22.10±5	1.2±0.21
GR–Polyimide	0.1	105.8±8	15.03±4.5	1.74±0.35
GR–Polyimide	0.5	113.8±7	14.5±2	2.13±0.42
GR–Polyimide	1.0	130.5±10	9.7±2.5	3.08±0.45

Table 3. Mechanical properties of the GR–PI composites, in comparison to other carbon filler composites.

Matrix	Filler–Wt%	Improved stress (%)	Improved Young Modulus (%)
PI[47]	FGS–0.38	7	30
PI[48]	CMG–1	30	46
PI[48]	GO–1	18.6	34
PI[49]	FGS–2	30	30.2
PI[50]	GCA–0.8	30.9	27.2
PI[51]	G–4	–	25–30
PP[52]	G–1.9[a]	–	43
GR–PI (our work)	**GR–1**	**54.8**	**156**

FGS: functionalized graphene sheet; CMG: chemically modified graphene; GO: graphene oxide; GCA: graphene carboxylic acid; G: graphene; a: volume%; PI: polyimide; and PP: polypropylene.

Figure captions

Figure 1. Schematic showing the method used to fabricate the solid array of ZnO/C core–shell hexagonal nanorods, highly dispersed conducting graphene ribbons (GR), and GR–polyimide (GR–PI) composite films. (a) Zinc oxide microparticles were prepared from zinc acetate dihydrate during the first stages of synthesis in a sealed bath. (b) ZnO/C core–shell hexagonal nanorods prepared by thermolysis in a sealed bath with heating at 450°C for 40 h. (c) The hexagonal and noncapped CNTs were formed by the removal of the core ZnO portion under HCl treatment. (d) GRs were produced by sonication of the noncapped CNTs in an HCl solution. (e) A GR–PI composite film was produced by adding PMDA and ODA to the GR solution in the NMP solvent.

Figure 2. (a) SEM image of a stack of ZnO/C core–shell hexagonal nanorods array. (b) High–resolution SEM image of the ZnO/C core–shell hexagonal nanorods shown in Figure (a) (side view). (c) SEM image of the tip of ZnO/C core–shell hexagonal nanorods (front view). (d) SAED pattern obtained from a ZnO/C core–shell hexagonal nanorod. (e) High resolution TEM image of ZnO/C core–shell hexagonal nanorods showing the transparent carbon–coated phase.

Figure 3. Raman spectra of (a) the non–reduced (as–prepared) GRs, and (b) the reduced (heated) GRs.

Figure 4. (a) SEM images of a stack of GRs. (b) SEM image of the GRs (side view). (c) Rectangular area of the GRs indicated in **Fig. 4b**. (d) TEM image of the GRs. The inset shows the SAED pattern. (e) TEM image of two individual GRs. (f) HR–TEM image of three–layer

GRs. (g) TEM image of one GR. (h) HR–TEM image of bi–layer GRs taken from the marked positions of (g).

Figure 5. SEM images showing the creation of GRs from ZnO/C core–shell structures through sonication in a 10% HCl solution. (a) Hollow CNTs were prepared by 3 min sonication. (b) The CNTs were partially unzipped by 4 min sonication. (c) The complete unzipping of the CNTs occurred within 5 min sonication.

Figure 6. Schematics showing the fabrication of a GR stack obtained from the ZnO/C core–shell hexagonal nanorods. (a) ZnO/C core–shell hexagonal nanorods. (b) ZnO dissolved to form $ZnCl_2$, leaving a hollow CNT structure, after the addition of 10% HCl and subsequent sonication. (c) The CNTs became unzipped during sonication. (d)–(f) Unzipped sheets turned into GRs during sonication. Photographs of (g) the GR solution containing 10 mg/mL GR in NMP after 14 days and (h) top 80% of the solution (1.95 mg/mL) collected from (g). The solution of (h) was found to be stable for more than 3 months.

Figure 7. Photographs of (a) a 1 wt% GR–PAA composite film, and (b) a 1 wt% GR–PI composite film. (c) Stress vs. strain% curves for films prepared from different wt% GR–PI composites or pure PI solutions. (Curve a) Stress–strain% curve for a pure PI film. (Curve b) Stress–strain% curve for a 0.1 wt% GR–PI composite film. (Curve c) Stress–strain% curve for a 0.5 wt% GR–PI composite film. (Curve d) Stress–strain% curve for a 1 wt% GR–PI composite film.

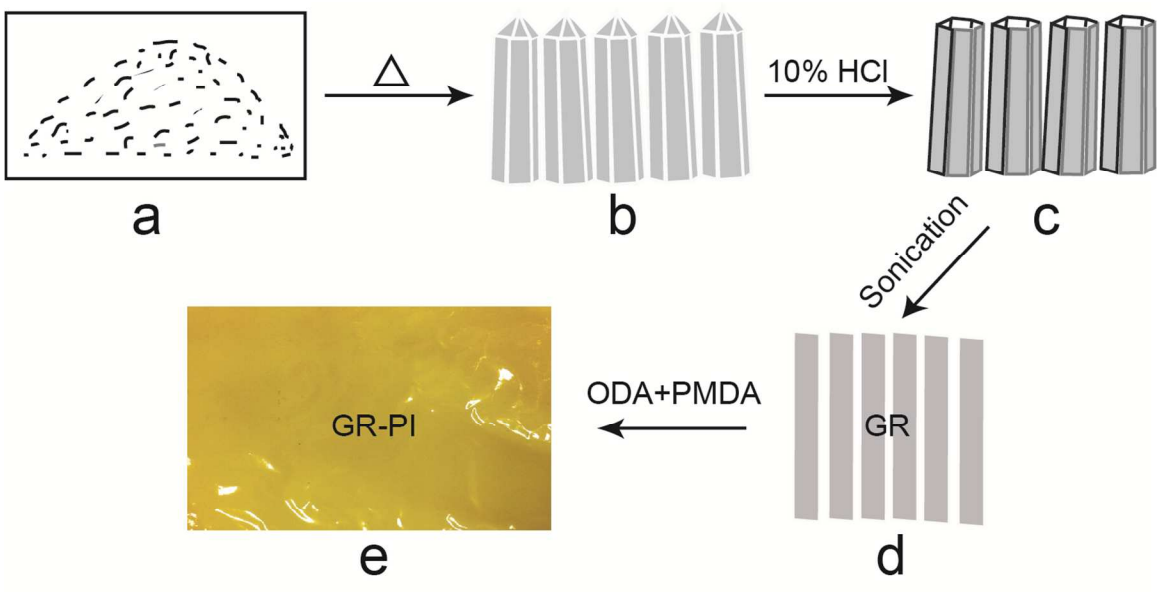

Figure 1

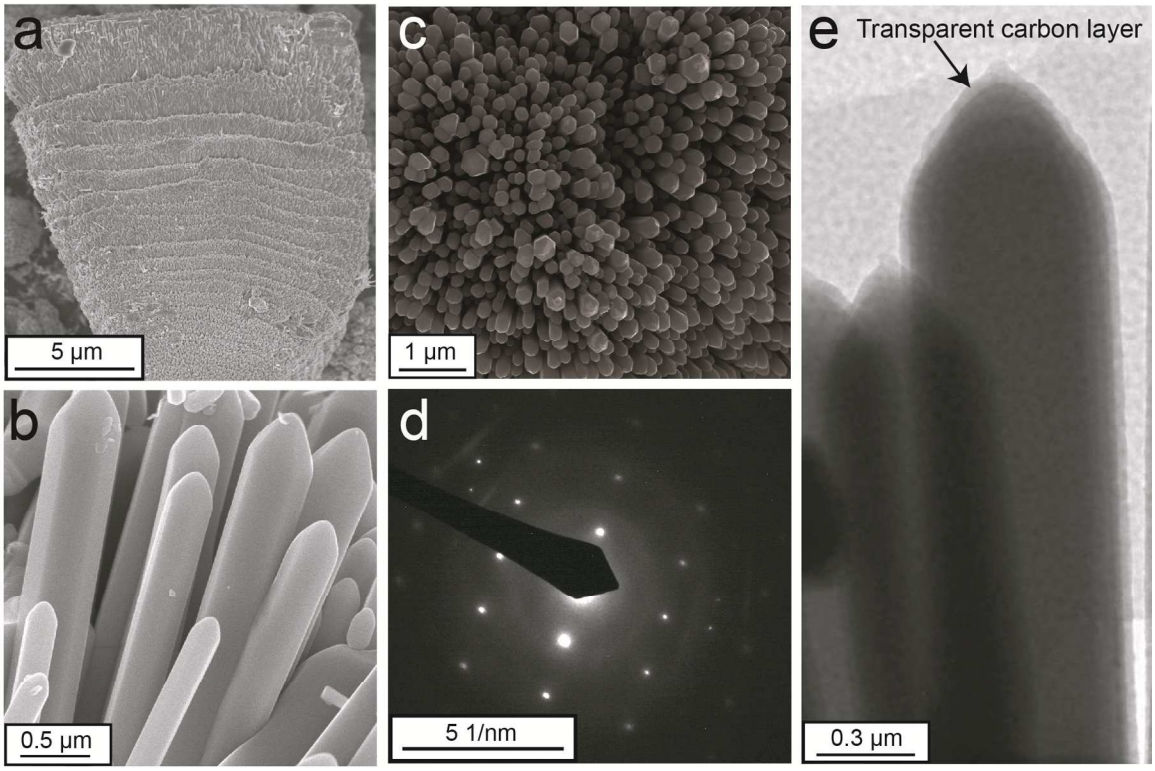

Figure 2

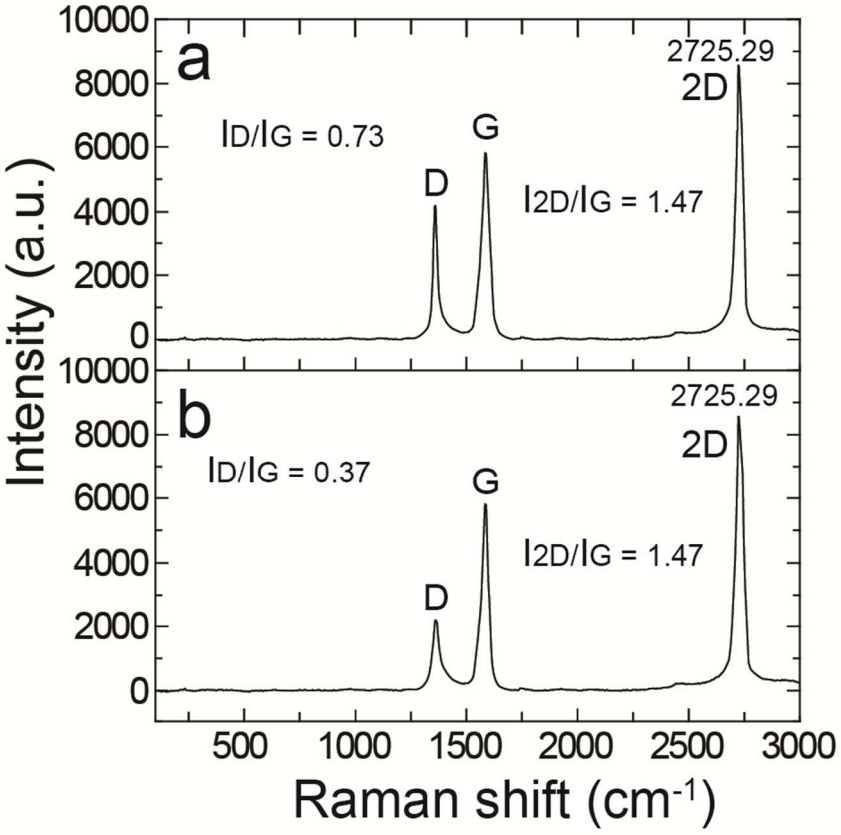

Figure 3

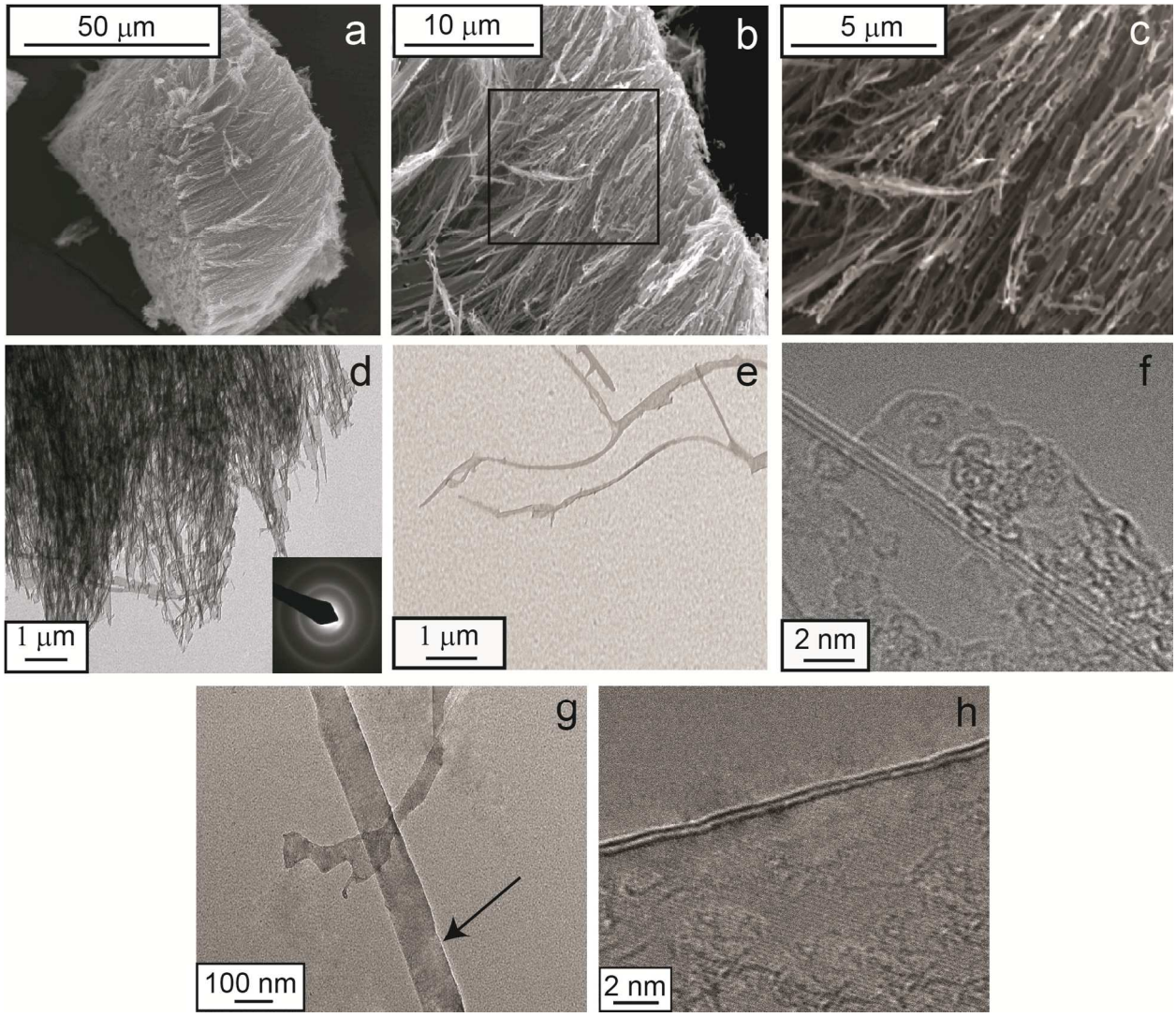

Figure 4

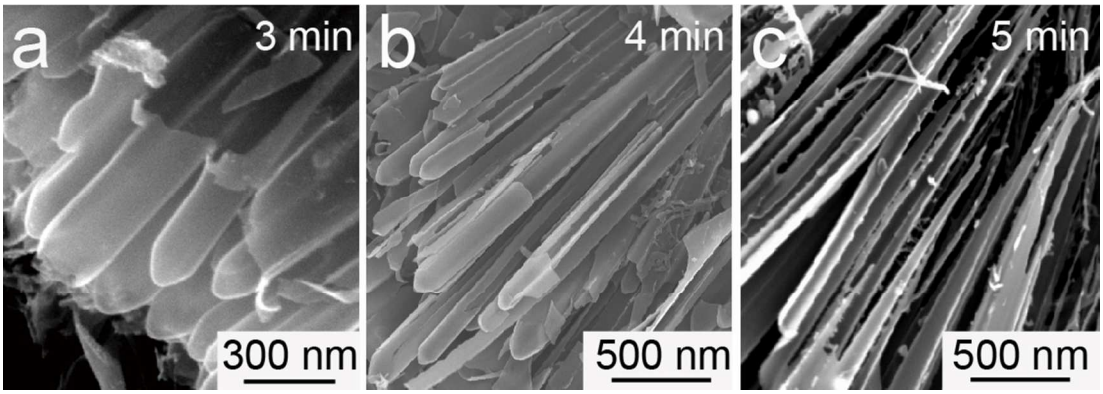

Figure 5

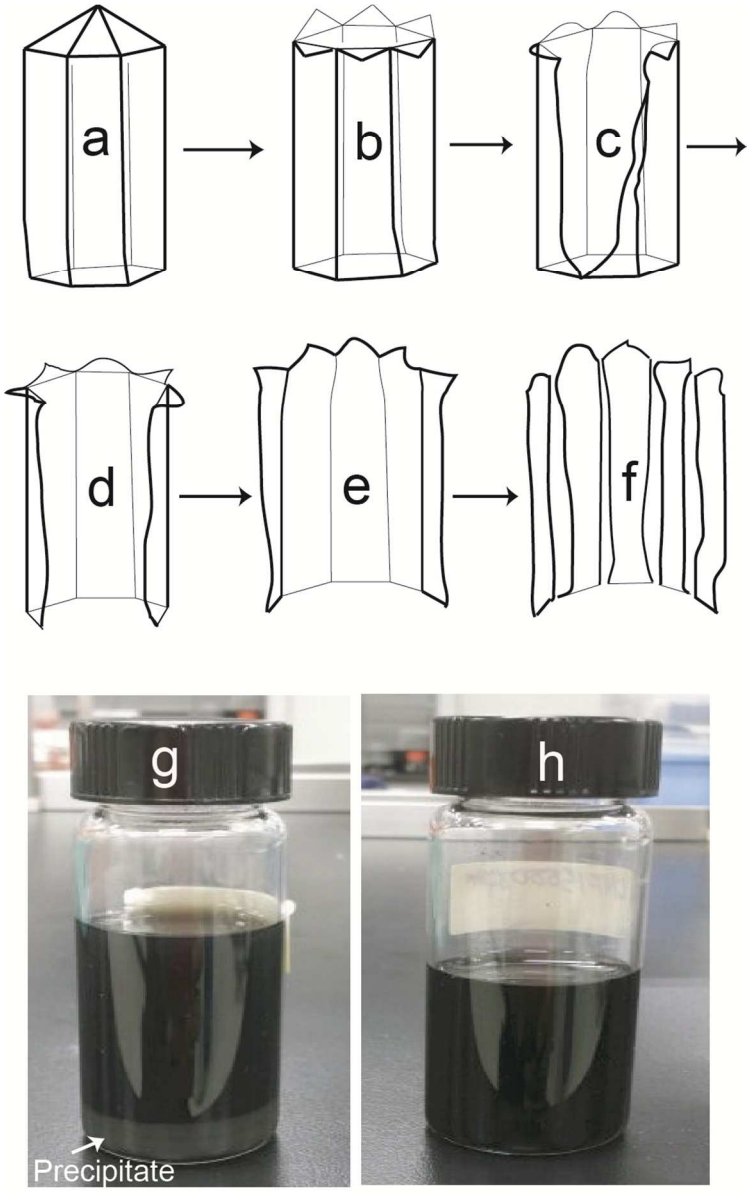

Figure 6

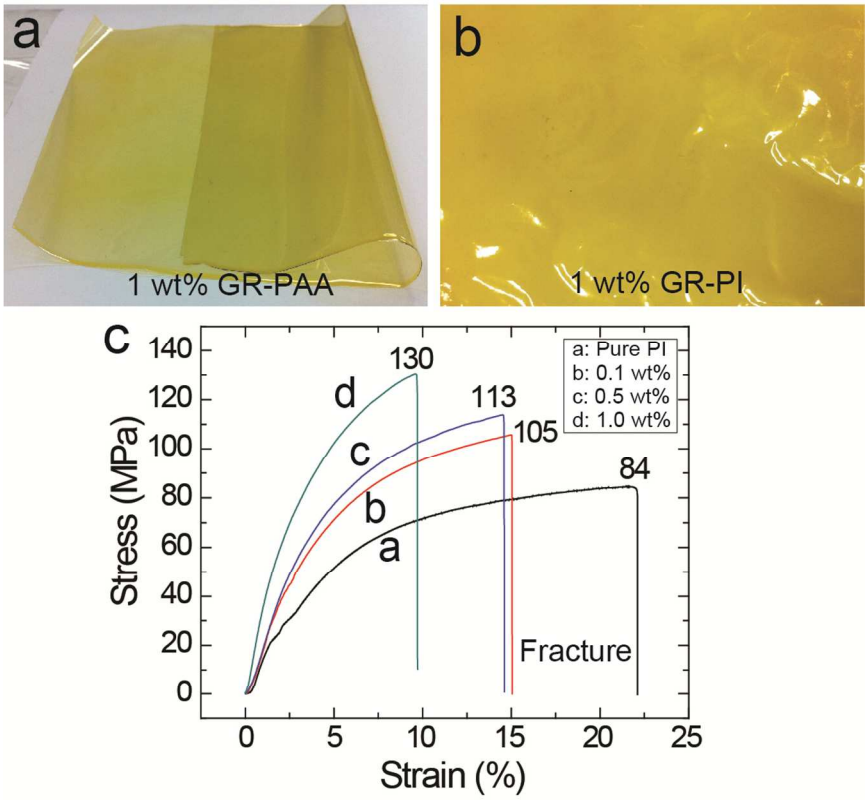

Figure 7

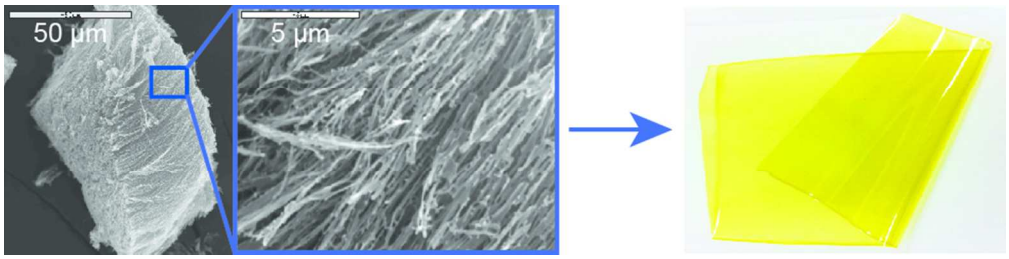

80x19mm (300 x 300 DPI)